Observations of Deep Convection in the Gulf of Lions, Northern Mediterranean, during the Winter of 1991/92

FRIEDRICH SCHOTT

Institut für Meereskunde an der Universität Kiel, Kiel, Germany

MARTIN VISBECK

Department of Earth, Atmosphere and Planetary Sciences, Massachusetts Institute of Technology, Cambridge, Massachusetts

UWE SEND, JÜRGEN FISCHER, AND LOTHAR STRAMMA

Institut für Meereskunde an der Universität Kiel, Kiel, Germany

YVES DESAUBIES

Laboratoire de Physique des Oceans, IFREMER, Plouzane, France

(Manuscript received 10 January 1995, in final form 16 June 1995)

ABSTRACT

During December 1991 to April 1992 measurements with moored acoustic Doppler current profiler (ADCP) stations and shipboard surveys were carried out in the convection regime of the Gulf of Lions, northwestern Mediterranean. First significant mixed layer deepening and generation of internal waves in the stratified intermediate layer occurred during a mistral cooling phase in late December. Mixed layer deepening to about 400 m, eroding the salinity maximum layer of saltier and warmer Levantine Intermediate Water and causing temporary surface-layer warming, followed during a second cooling period of late January.

During a mistral cooling period from 18 to 23 February 1992, convection to 1500-m depth was observed, where the size of the convection regime was 50–100 km extent. Vertical velocities 40–640 m deep, recorded by four ADCPs of a triangular moored array of 2 km sidelength in the center of the convection regime, exceeded 5 cm s^{-1} and were not correlated over the separation of the moorings. Horizontal scales estimated from event duration and advection velocity were only around 500 m, in agreement with scaling arguments for convective plumes. Plume activity during nighttime cooling was larger than during daytime. Significant evidence for rotation of the plumes could not be found. Overall, plume energy, and the degree of mixing accomplished by them, was much lower than observed during a stronger mistral in February 1987.

The mean vertical velocity over the mistral period, determined from the four ADCPs, was near zero, confirming the role of plumes as mixing agents rather than as part of a mean downdraft in a convection regime. The cyclonic rim current around the convection regime was confined to a strip of <20 km width with an average velocity of about 10 cm s^{-1}, which is in agreement with near-zero vertical mean velocity in the interior based on potential vorticity conservation. A relation between variations of the larger-scale cyclonic North Mediterranean Current along the boundary and the deep convection could not be identified. An unexplained feature still is the cover of the convection regime by a shallow layer of light water that moves in rather quickly from the sides after the cooling ends.

1. Introduction

The Gulf of Lions, northwestern Mediterranean, is a region where deep convection occurs during most winters and, beginning with the now-classic MEDOC experiment 1969 (MEDOC Group 1970), the presence of near-homogeneous water bodies in the region has been documented several times (e.g., Gascard 1973, 1978; Leaman and Schott 1991). As the early MEDOC studies already showed, the situation leading to deep convection in the northwestern Mediterranean has as its basis the permanently present cyclonic structure of the circulation in the Gulf of Lions: the North Mediterranean Current (NMC) flows westward along the French coast, supplied in the east by two current branches that pass on both sides of Corsica (Astraldi and Gasparini

Corresponding author address: Prof. Friedrich Schott, Institut für Meereskunde, Universität Kiel, Düsternbrooker Weg 20, D-24105 Kiel, Germany.
E-mail: fschott@ifm.uni-kiel.d400.de

1992). In the west, the NMC partially continues southward along the Spanish coast, partially it turns offshore and recirculates eastward around the Gulf of Lions. This cyclonic circulation leads to a doming of the isopycnals with shallowest mixed layer depths in a band along about 42°N. Underneath, and separated from the surface by a layer of warmer, saltier Levantine Intermediate Water (LIW) in the depth range 300–600 m, lies the weakly stratified Western Mediterranean Deep Water (WMDW). The second essential ingredient is the occurrence of cold and dry winds that blow from the land over the isopycnal dome: the mistral out of the Rhone valley and the Tramontane from the Pyrenees. With continued cooling during the early phase of winter, the upper layer continues to cool, deepen, and entrain water from below. Finally, typically around mid-February, stability against the weakly stratified sublayer is reduced enough for deep convection to set in, in conjunction with mistral or Tramontane events. In early winter, the distribution of increased surface salinity caused by the upward mixing of LIW (easily measured by shipboard thermosalinograph) is a good indicator of the region where deep convection may occur later in the winter season.

For nearly two decades after the early MEDOC experiments, lack of technical innovation to measure vertical currents with moored instrumentation prevented studies of the detailed small-scale processes associated with deep convection. The first experiment with moored acoustic Doppler current profilers (ADCPs), carried out by Schott and Leaman (1991, henceforth called SL91) in the Gulf of Lions in 1987 showed that small-scale convection cells ("plumes") may occur when an existing deep-mixed regime is cooled again at the top. From the time that it took for a plume to be advected past the ADCP station by the mean flow, SL91 estimated the horizontal scale at <1 km. Subsequent tank experiments (Coates et al. 1995; Maxworthy and Narimousa 1994) and nonhydrostatic numerical modeling (Jones and Marshall 1993) supported the existence of such small-scale plumes in homogenized convection regions during the presence of surface cooling. These studies also suggested the importance of rotation in constraining the horizontal scale of the plumes. However, the laboratory models obtain a much larger depth of the mixed layer at which the rotational control becomes effective than the numerical model simulations. Scaling arguments were developed that provided a dependence of the horizontal scale and downward plume velocity on two external parameters, rotation and surface buoyancy flux. Vorticity conservation would require that rotationally controlled plumes rotate cyclonically on top and anticyclonically at depth. The overall effect of convection within the deep-mixed regime should lead to enhanced cyclonic upper-layer rotation around the entire convection domain and anticyclonic rotation at depth, which was observed both in nonhydrostatic (Jones and Marshall 1993) and hydrostatic (Madec et al. 1991) models. On the other hand, vorticity conservation at the scale of the convection region requires that only small net downwelling should exist in the interior. Consequently, plumes should only act as mixing agents rather than transporting water masses downward in a mean motion (Send and Marshall 1995).

In 1987, when the convection studies of SL91 and Leaman and Schott (1991, hereafter LS91) were begun on 20 January, a previous mistral, occurring during 10–12 January, had already caused a deep-mixed regime of >50 km horizontal extent. The convection region shrunk during the calm weather of early February and expanded again by a second mistral during 17–23 February to the extent marked in Fig. 1, that far exceeded the size of the deep-mixed regime (then called "chimney") observed during MEDOC 1969 (Fig. 1). In the ADCP observations of SL91, a mean downward motion of about 1 cm s^{-1} in that deep-mixed regime was measured at the one ADCP position over the one-week duration of the mstrali cooling period, which was considered significantly different from zero and used to infer a mean downward transport in the convection regime.

A similar study with moored ADCPs in the central Greenland Sea in winter 1988/89 (Schott et al. 1993) yielded more details on the convection processes. Similar to the Gulf of Lions, preconditioning there is achieved by cyclonic circulation around the central Greenland Sea combined with upward mixing of warmer saltier intermediate waters of Atlantic origin and subsequent mixed layer cooling. In late winter, developing out of a homogenized mixed layer pool of about 400-m depth and 50-km extent in the central Greenland Sea, plumes were observed down to 1400 m by moored ADCPs during an intense cooling phase. In contrast to the findings of SL91 though, vertical mean currents during the convection phase, measured by three ADCPs at different positions and depths, were zero and the plumes did not mix the depth range 400–1400 m to a homogeneous water body. Hence, in contrast to the complete mixing case of 1987, this was a case of incomplete mixing by the plumes. Another observation at both convection sites was that density steps were not observed in CTD profiles at the bottom of the convective regime, indicating that plume mixing was nonpenetrative in those cases.

During 1991/92 a new convection experiment was carried out in the Gulf of Lions (THETIS Group 1994). The experiment included an acoustic tomography array (T1–T6, Fig. 1), deployed from December to late April to use acoustic ray propagation for mapping stratification changes associated with convection (Send et al. 1995). A triangular ADCP array of 2-km sidelength was located in the center of the potential convection regime (A1, A2, T6; set in Fig. 1). One of the moorings

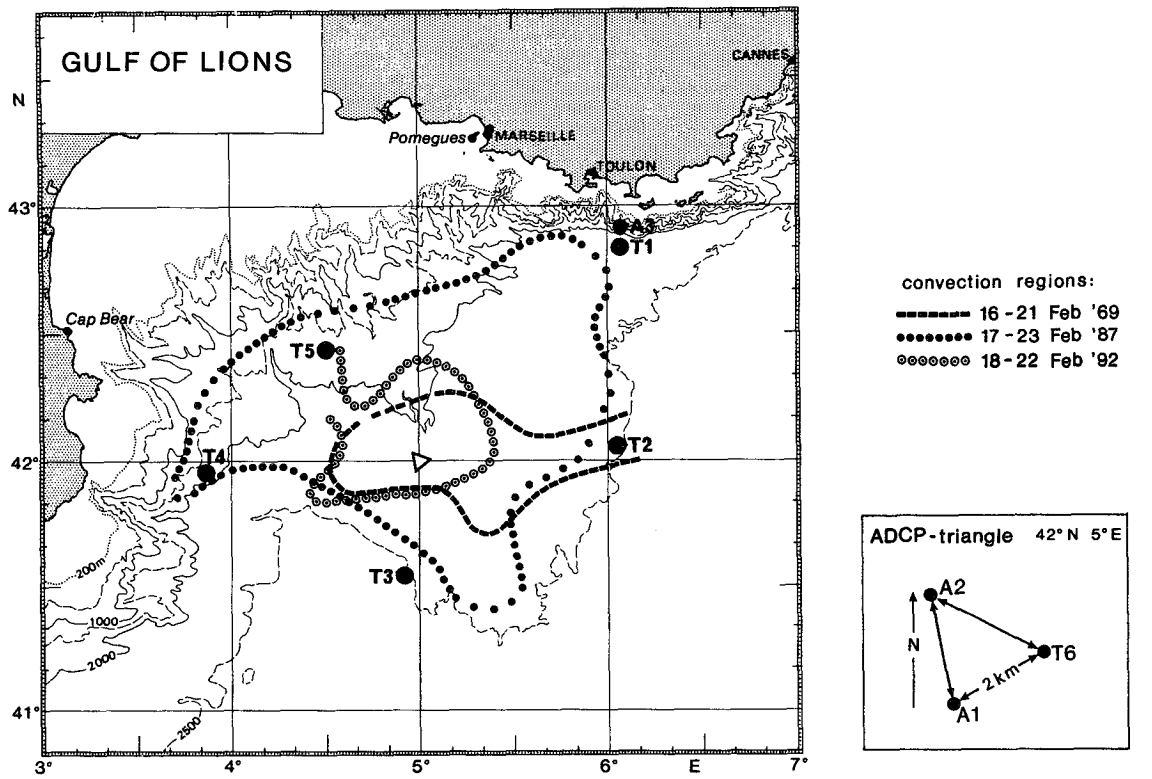

FIG. 1. Topography of the Gulf of Lions and positions of moored stations (for small-scale triangle see inset); also marked are boundaries of deep-mixed regions in Februaries of 1969, 1987, and 1992.

was also equipped with thermistor strings and conductivity recorders for stratification measurements. Further, two moorings were deployed in the northern boundary current (A3, T1, in Fig. 1) to measure horizontal currents and transport variations that might occur around the convection regime in conjunction with the above described circulation changes. The tomography moorings (T2–T5, Fig. 1) also carried additional current and temperature recorders at selected depths. Shipboard surveys (by three research vessels, the French vessel *Le Suroit* of IFREMER, as well as the German vessels *Poseidon* and *Valdivia*) were carried out several times during the deployment period. The *Poseidon* survey happened to fall into the main mistral cooling period during 18–23 February, and small-scale CTD measurements (tow-yos) were carried out in the convection zone in an attempt to map changes at the plume scale.

From the tomography inversions of Send et al. (1995), it was estimated that the convection due to the mid-February 1992 mistral mixed an area of approximately 60-km radius to a mean depth of about 1500 m, corresponding to an annual deep water renewal rate of 0.3 Sv (Sv $\equiv 10^6\ m^3\ s^{-1}$). A similar estimate was obtained by Rhein (1995) from Freon-F11 and F12 budget calculations for the convection region. In the present paper we will address the development of atmospheric forcing over the winter 1991/92 and the corresponding changes in stratification and water mass properties, which are spatially much more inhomogeneous than in the "super-mistral" year of 1987. We will then discuss the changes of mean circulation and mesoscale variability associated with the occurrence of deep convection. Finally, the vertical velocities observed by the small-scale ADCP mooring array are presented, and we conclude on their spatial structures.

2. The moored and shipboard measurements

In the triangular array in the center of the convection regime, one mooring, station A1, was equipped with two ADCPs. One was looking upward toward the surface from 300 m; the second one was located just underneath and looking downward. Combined, they provided a joint vertical measurement range of about 600 m. Temperature stratification of the upper several hundred meters at station A1 was recorded by two thermistor strings. One covered the range 50–250 m at 20-m resolution; the second one the range 340–740 m at 40-m resolution. However, the thermistor strings

stopped recording in early February 1992. Although they thus missed the major convection event described in the following, the cooling episodes of the preconditioning phases were still well documented. For conductivity/salinity recordings, station A1 was equipped with four Seacat recorders at 322-, 1002-, 1400-, and 1802-m depth.

The other two moorings of the central array, A2 and T6, were each equipped with one ADCP looking downward from 300 m to observe horizontal structures at the 2-km scale during convection activity. From the SL91 and Schott et al. (1993), estimates of horizontal scales from advection timescales, as well as from the scaling arguments recently advanced, it was to be anticipated that the array spacing of 2 km might be too large to resolve plumes. However, array resolution might be sufficient at a later stage when deep-reaching baroclinic eddies, to be expected from modeling results (Jones and Marshall 1993), had developed.

The nominal vertical bin length of the upward looking instrument (A1U) was 8.8 m; for the three downward-looking ADCPs (A1D, A2, T6), it was 17.6 m. To resolve the fluctuations in the period range of an hour or so, the ensemble time interval for the ADCP sampling was set at 12 min, with 125 pings per ensemble. All four ADCPs delivered good data for the entire recording period. The various recorded attitude parameters (pitch, roll, orientation) as well as depth (evaluated from the traveltime of the surface backscatter signal) showed that the instruments were sitting still in the water with only small vertical excursions, only low rotations around their vertical axes, and small inclinations during individual deep-reaching horizontal-current events. Below the ADCPs, rotor current meters (Aanderaas) were deployed at 1000 and 1800 m, where the purpose was to observe the change of vortex rotation with depth, should rotating plumes or eddies with resolvable scales pass the array.

Cruises in the convection region were carried out by three research vessels. There were three cruise legs by *Le Suroit,* during 26 November–7 December 1991, 7–16 January 1992, and 11–24 April 1992. *Valdivia* worked during 7–23 December 1991, and *Poseidon* during 18 February–10 March 1992. *Poseidon* and *Valdivia* were equipped with a Neil Brown CTD and rosette, as well as a shipboard ADCP, while *Le Suroit* employed a Seabird CTD, although without water sampling, and also was without an ADCP. Water mass studies by Freon analysis were carried out on the *Valdivia* and on *Poseidon* cruises (Rhein 1995).

The moored arrays were deployed during the November/December 1991 cruises of *Le Suroit* and *Valdivia* and retrieved in April 1992 by *Le Suroit.* Due to malfunctioning of the tomographic instruments (THETIS Group 1994), all of the stations T1–T3, T5–T6, and A2 had to be retrieved in February for repair, which caused some gaps and instrument position changes and also reduced the time that could be spent on shipboard surveys of the convection regime in February.

3. Development of stratification and deep convection

a. Meteorological conditions

The meteorological stations at the coast (Fig. 1) that well indicate the presence of the mistral and Tramontane winds, are Pomegues and Cap Bear, respectively (SL91). Wind vectors for both stations are shown in Fig. 2a, air temperatures in Fig. 2b. Also shown are the corresponding data and heat flux components (Fig. 2c) from the French *Peridot* model for a grid point near the small-scale mooring triangle. The model data are available as 12-h averages; horizontal resolution is 20 km. Comparisons with estimates from shipboard meteorological measurements during the *Valdivia* and *Poseidon* surveys showed significant biases in the latent and sensible heat flux components of the Peridot model, resulting from an underestimation of wind speed. In the total heat budget, this underestimation is nearly compensated by an overestimation of outgoing longwave radiation. This disagreement has also been found for annual averages over the western basin by Martel and Martel (1994), in a comparison of Peridot heat fluxes with those from other sources (e.g., Garrett et al. 1993). A mean correction of 15 W m^{-2} has been applied to the longwave radiation in Fig. 2c for better agreement with the mean shipboard fluxes. For individual mistral cooling episodes, the correction to both sensible and latent heat flux components in the Peridot time series (Fig. 2c) was estimated at about 30%.

Several events of strong winds blowing from the land over the Gulf of Lions occurred during the winter of 1991/92: The first strong wind period of the season happened at both coastal stations during 17–30 December, with a brief pause during 26–28 December. Peridot wind stress shows a pattern similar to the Pomegues land station. During the first part of this strong wind episode, the temperatures actually show a warming trend and then drop but not too much below the initial temperature. Yet, due to the high wind speed, the sensible and latent heat loss in the model total more than 400 W m^{-2} during three days of the strong wind phase. The second period of strong offshore winds occurred during 22–23 January. This event was accompanied by near-zero temperatures at Cap Bear but not at Pomegues, while Peridot temperatures over the measurement area showed a minimum of 8°C, and consequently Peridot heat loss reached only 350 W m^{-2}.

During 18–23 February, a mistral event with coastal night temperature minima near 3°C occurred, expressed by two 400 W m^{-2} heat loss maxima in consecutive nights in the Peridot model data. Subsequently, temperatures increased steadily with increasing solar radiation until another cooling period during 24–30

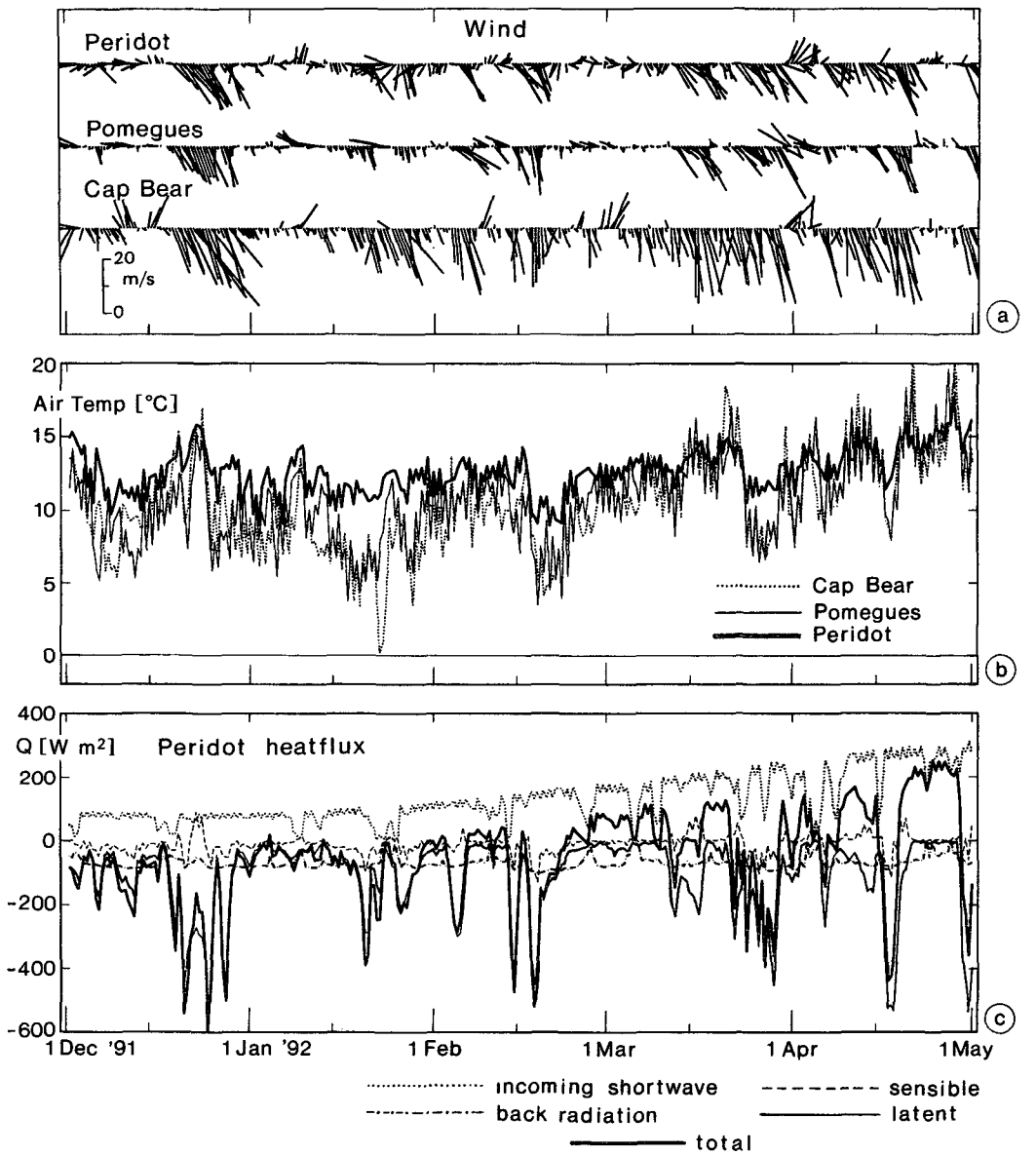

FIG. 2. (a) Time series for December 1991–April 1992 of wind vectors (direction towards) for coastal stations Cap Bear and Pomegues, and for "*Peridot*" model at 42°N, 5°E; (b) same as (a) but for air temperatures. (c) Heat flux components and total heat flux of "*Peridot*" model.

March interrupted the seasonal warming. The final cooling episode of up to 600 W m^{-2} heat loss occurred during 20–24 April—that is, shortly before the end of the recording period of our mooring triangle. As mentioned above, the cooling spikes in Fig. 2c would need an addition of about 30% for agreement with other measurements.

b. Development of stratification

Several ship CTD surveys were carried out during late November 1991 to April 1992. The initial CTD surveys by *Le Suroit* and *Valdivia* showed the well-known preconditioning dome with its elongated center along approximately 42°N. A meridional section through the dome along 5°E demonstrates the doming of potential temperature (Fig. 3a) and of isopycnals (Fig. 3b) with a maximum elevation of the dome just north of 42°N. The temperature maximum of the LIW is present across the entire section (Fig. 3a). This stratification stayed intact through January, as documented by a large-scale survey of the region carried out by R/V *Le Suroit*. However, mixed layer density had in-

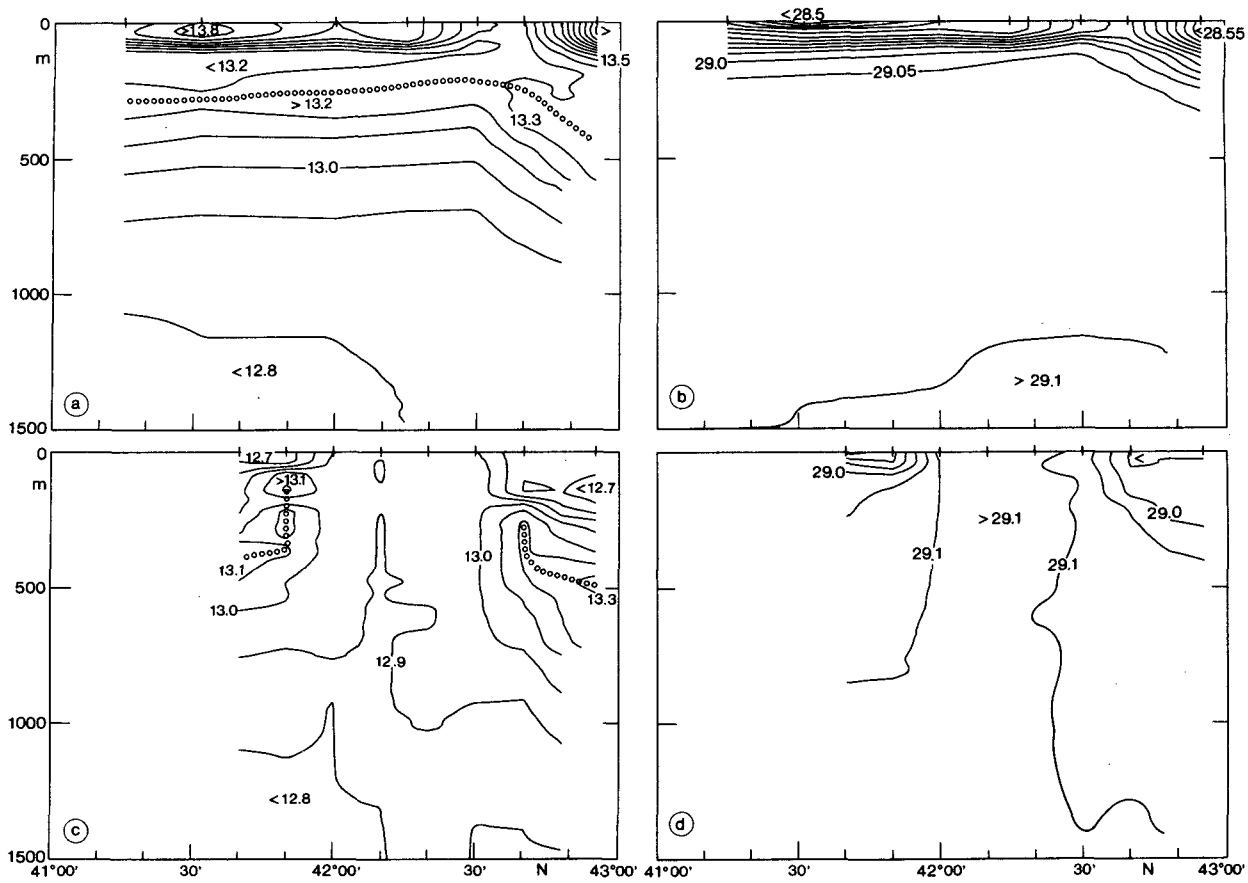

FIG. 3. (a) Sections along 5°E of potential temperature (with LIW temperature maximum indicated by open circles) for 12–18 December 1991. (b) Potential density for 12–18 December 1991. (c) As in panel a but for 20–22 February 1992. (d) As in panel b but for 20–22 February 1992.

creased by that time and the mixed layer in the center of the dome had deepened. Warmer, more saline LIW had been mixed upward and cooled. As a result, the stability to the weakly stratified deeper layers had been reduced.

At the time of the next survey, by R/V *Poseidon,* a near-homogeneous water body was found along that same section (Figs. 3c,d) between 42°00′N and 42°30′N. The potential temperature distribution for 20–22 February 1992 (Fig. 3c) shows an almost complete "chimney" of water colder than 13.0°C between about 1000-m depth and the sea surface at about 42°10′N. The temperature maximum of the LIW was slightly reduced and tilted upward at the northern end of the convection region. Although along the entire section the surface density increased compared to December, the density stratification was eroded (Fig. 3d) only over a restricted part of about 50 km extent north of 42°N.

From the CTD profiles, combined with XBT and XCTD data, the spatial distribution of the convection was determined for the periods 18–22 February (Fig. 4a), 23 February–2 March (Fig. 4b), and 3–9 March (Fig. 4c). The convection depth was identified by the extent of the profiles for which the potential temperature was vertically constant within ±0.05°C. This potential temperature range is larger than the 0.02°C used by Swallow and Caston (1973), but in 1969 the convection was more homogeneous than in 1992. In the CTD casts, a temperature step at the bottom of the homogeneous part of the profile was accompanied by a salinity step with both steps largely compensating in density. In March, a few CTDs showed two convection depth layers with a temperature offset of more than 0.05°C. In this case both layers were regarded as convection regimes. As the CTD measurements often started a few meters below the sea surface, gradients in the upper few meters were neglected.

During 18–22 February 1992 (Fig. 4a) the extent of the mixed patch along 5°E reached from 41°50′N to 42°25′N, thus covering the ADCP array near 42°N (Fig. 1). The mean potential density of the deep-mixed

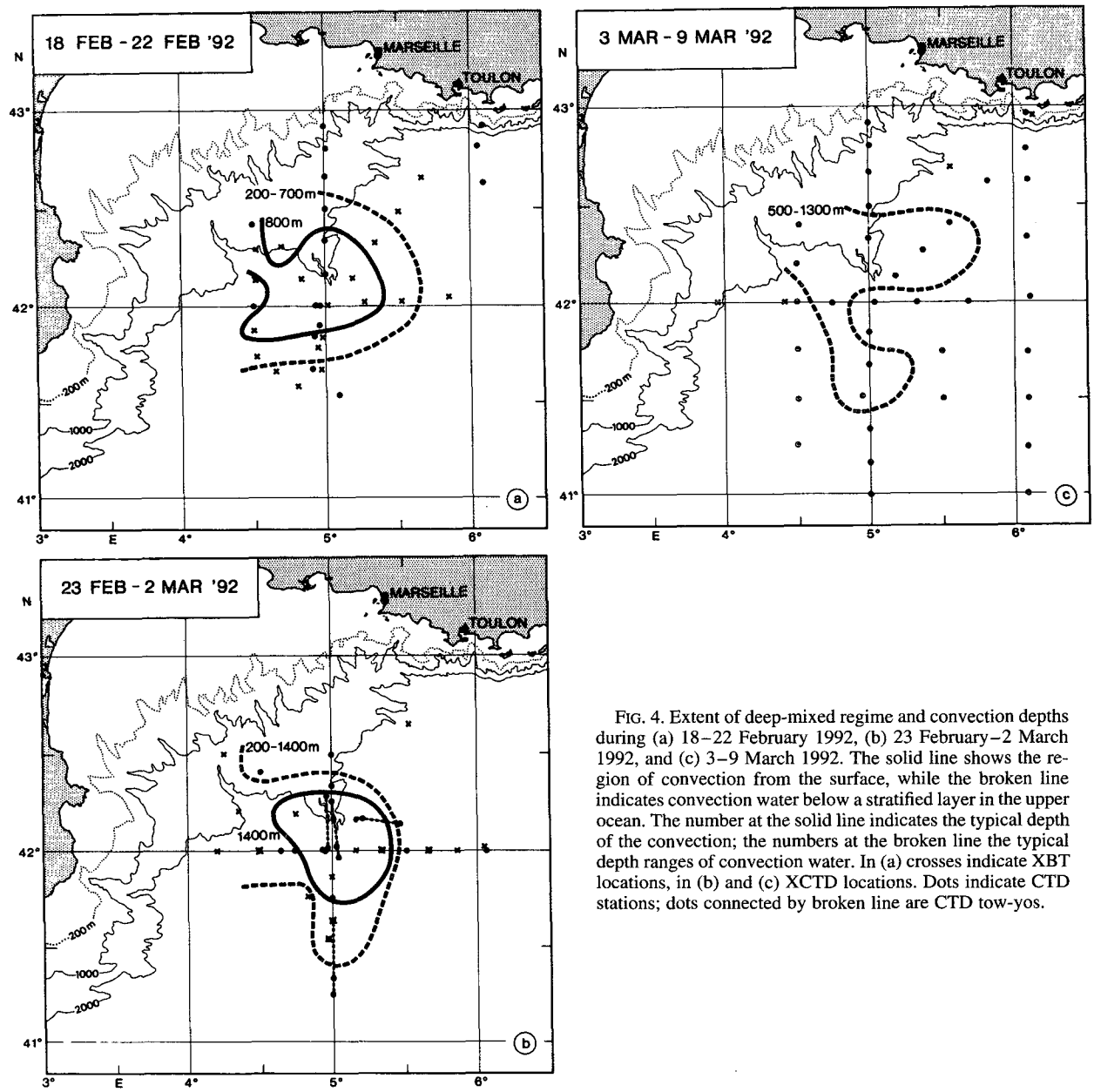

FIG. 4. Extent of deep-mixed regime and convection depths during (a) 18–22 February 1992, (b) 23 February–2 March 1992, and (c) 3–9 March 1992. The solid line shows the region of convection from the surface, while the broken line indicates convection water below a stratified layer in the upper ocean. The number at the solid line indicates the typical depth of the convection; the numbers at the broken line the typical depth ranges of convection water. In (a) crosses indicate XBT locations, in (b) and (c) XCTD locations. Dots indicate CTD stations; dots connected by broken line are CTD tow-yos.

stations was 29.100, with the slight inversion above 800 m indicating continuing buoyancy flux (Fig. 5a). Potential temperature within the deep-mixed patch was 12.95°C and salinity 38.48 (Fig. 5a). Except for the northwest, where the CTD stations did not reach far enough coastward to locate the edge of the patch, the convection region was surrounded by a regime of about 25-km width, where convection water was observed below a surface stratified layer, typically in the depth range 200 to 700 m (Fig. 4a). At this time the typical convection depth within the patch was 800 m (Fig. 5a), with two stations reaching 1000 m.

In the following days, 23 February to March 2 (Fig. 4b), the convection reached down to 1500 m depth with a typical depth of 1400 m, centered again at 42°N, 5°E. The patch mean potential density had increased to 29.104 (Fig. 5b), the potential temperature was 12.88°C, and the salinity 38.47. The surrounding ring of convection water, disconnected from the surface (typically between 200 and 1400 m) extended mainly to the south and west, while to the north and east this region was very limited. In the week of 3 to 9 March (Fig. 4c), no homogeneity was clearly observed up to the sea surface. Only the

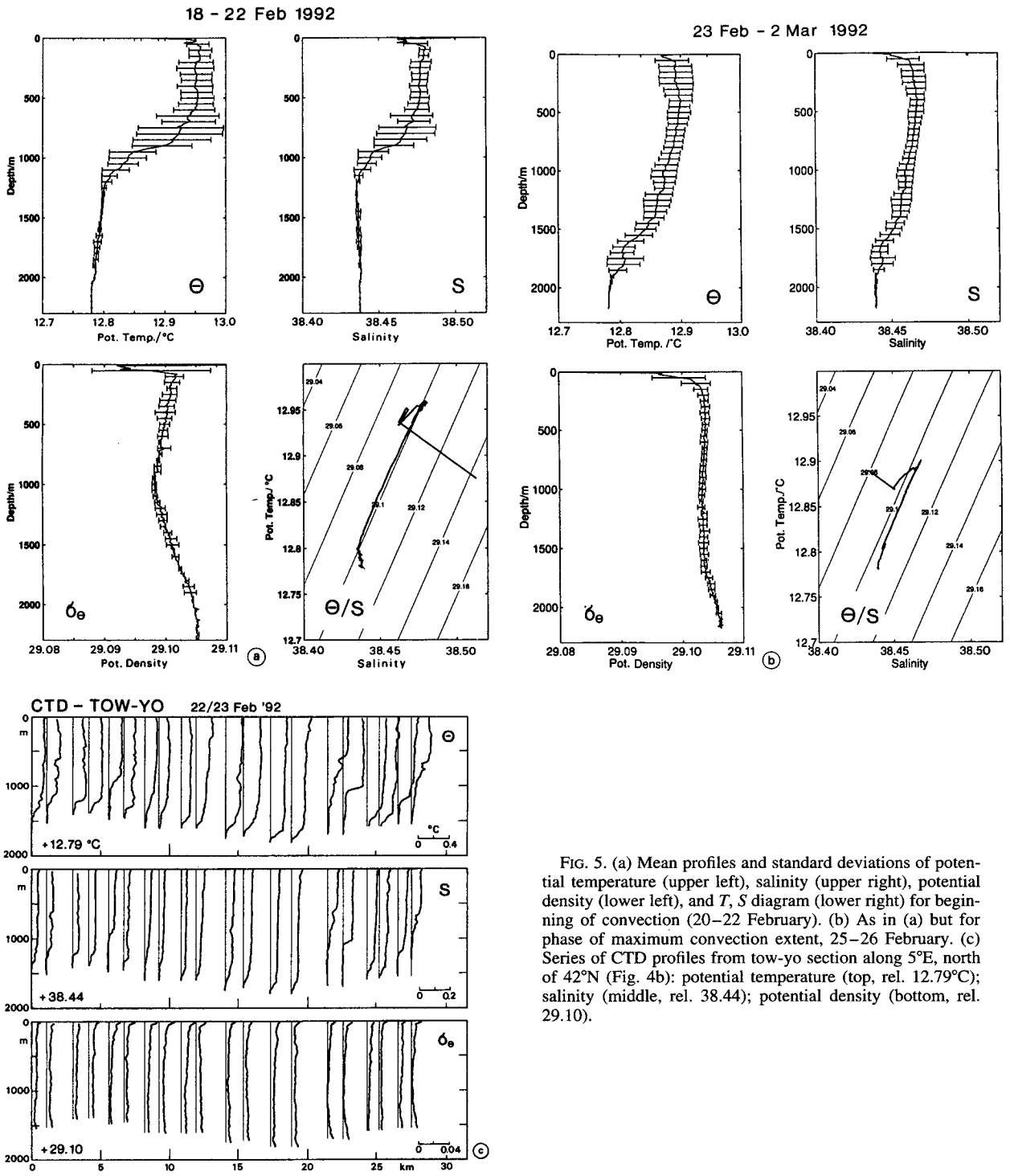

FIG. 5. (a) Mean profiles and standard deviations of potential temperature (upper left), salinity (upper right), potential density (lower left), and T, S diagram (lower right) for beginning of convection (20–22 February). (b) As in (a) but for phase of maximum convection extent, 25–26 February. (c) Series of CTD profiles from tow-yo section along 5°E, north of 42°N (Fig. 4b): potential temperature (top, rel. 12.79°C); salinity (middle, rel. 38.44); potential density (bottom, rel. 29.10).

northwestern station at 42°20′N, 4°30′E showed a disturbed convection profile between 50 and 1500 m. In the interior, remainders of the convection were typically found between 500- and 1300-m depth. This layer was most pronounced to the northeast and south, while at the center of the previous convection, at 42°N 5°E, no convection water was present. The regimes indicated by the dashed lines compare well

with the estimates from the tomography array (Send et al. 1995).

The depth and composition of the convection patch in 1992 was quite different from the 1987 case. The mixing in 1992 only reached to approximately 1500-m depth, compared to 2200 m in 1987. Further, the 1992 convection was a case of "incomplete mixing," because significant differences in water mass properties among closely spaced stations were observed in CTD "tow-yos" (Fig. 5c). While the potential density of the convection water was 29.102–29.103 in that small tow-yo segment through the convection patch, the ranges in temperature, at 12.87–12.98°C, and salinity, at 38.45–38.48, were quite substantial, compared to the near-homogeneity in 1987 (LS91). Similarly, the profile standard deviations in Figs. 5a,b are large in T and S, while small in σ_θ.

The convection, as observed in the CTD profiles, did not show signs of entrainment at the bottom of the homogeneous layers; that is, although steps in the salinity and temperature profiles were frequently observed, density steps were not (e.g., Fig. 5c). Hence, convection was nonpenetrative, as already observed earlier in that convection regime (Anati 1971; LS91).

A yet poorly documented and not understood phenomenon following convection periods, especially under weak meteorological forcing conditions is the moving in, from the sides, of a thin stratified surface layer of warmer water. This "capping" was previously described by LS91 and SL91 in relation to the drastic shrinking of the surface area occupied by convection water during weak winds of late January to early February of 1987. Due to the surface trapping of the acoustic rays for all possible stratifications in the Gulf of Lions the tomography experiment was particularly useful for measuring the capping; and, as shown by Send et al. (1995), the intrusions of warm surface waters filled wide parts of the convection patch of Fig. 4. The capping was destroyed again by the cooling period of late March (Fig. 2c). The mixed layer model runs of Mertens (1994) that yielded good agreement of the seasonal development of convection depth and convection temperature with the observations until February failed to reproduce the capping, thus supporting the conclusion that it is caused by lateral advection. From the CTD profiles as well as the near-surface ADCP data no satisfactory results on the physics of the capping processes could be gained, so far.

The temporal development from December to February, leading to deep convection, can be seen from a contour plot of thermistor string temperatures recorded during the preconditioning phase, through early February, at station A1 in the depth range 50–740 m (Fig. 6a), and from the time series of temperature and salinity from several depths between 50 and 1800 m at that

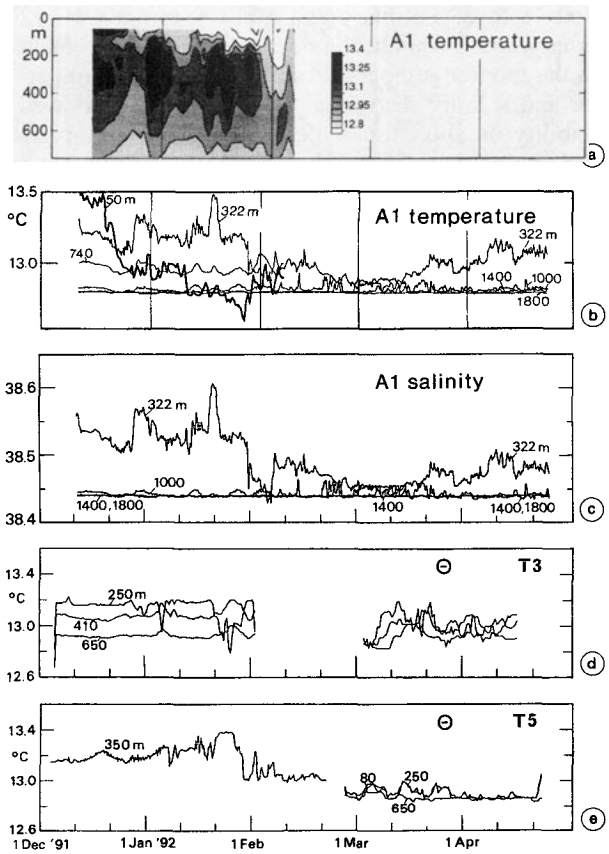

FIG. 6. (a) Potential temperature contour plot from thermistor string recordings for preconditioning phase for upper 650 m at station A1. (b) Potential temperature time series for several depths at station A1. (c) Same as in panel b but for salinity. (d) Same as in panel b but for station T3. (e) Same as in panel b but for station T5.

station over the entire observation period (Figs. 6b,c). The first cooling episode in late December (Fig. 2c) caused the 50-m temperature to drop by 0.5°C below the LIW temperature (Fig. 6b) and resulted in approximate homogeneity to about 150 m. Then restratification set in at that station, which was located at the southern front of the convective patch, until late January when another mixing event occurred, this time reaching to deeper than 400 m (Fig. 6a). During this event the 322-m salinities decreased by 0.1, even below the lower-level salinities (Fig. 6c). The deep records show that homogeneity reached the 1000-m level on 19 February and the 1400-m level on 22 February, when the temperatures at these levels jumped from the deep water value of 12.80°C to the mixed layer temperature of 12.90°C. Simultaneously, the 1000-m salinity approached that of the 322-m record (Fig. 6c). Small differences, within the calibration accuracy of the sensors, remained between the 322-, 1000-, and 1400-m records. Although the CTD survey showed only typical convection depths of about 800 m for the

period 18 to 22 February and of 1400 m between 22 February and 2 March, the deepening is in agreement with the moored temperatures. As the 1000 m temperature and salinity records at A1 (Figs. 6b,c) showed variability on short timescales, the shallower convection depth of the CTD might have been observed at a time when a temperature change occurred above 1000 m at A1. After about 15 March, the upper-layer mooring temperature increased again, but, at the deep levels, temperature variance continued to be higher than before the winter season throughout April.

At the southern periphery of the convection regime, station T3, the thermistor string temperatures from the 250 to 650 m range, which have an interruption due to data storage problems and station exchange from 29 January to 1 March, show that near-homogeneity occurred briefly at the beginning of the second recording period, until 5 March, and again around 15 March (Fig. 6d). This indicates that T3 was at times within and at times outside the convection regime. At station T5, the warming at 350 m during December and January shows that warmer LIW was entrained upward (Fig. 6e). Then, around 25 January, drastic cooling occurred, indicating that the mixed layer depth had passed the LIW temperature maximum. Thermistor string records from after 25 February at position T5 show near homogeneity between 250 and 650 m from late March until the end of the recording period. Since T5 was the station with the thickest layer of convection water in the 3–9 March ship surveys, these records indicate better the duration of the deep mixing of the patch than T6/A1 at the periphery (Fig. 4c). Further, the tomography inversions of Send et al. (1995) show that most of the line connecting T6 and T5 (Fig. 1) was then still occupied by water masses of deep-mixed characteristics. This result supports the conclusion that the water body formed by convection stayed intact for at least the following two months in the northern region where it is pushed against the topography and thus poses more difficulty for lateral eddy exchange. Figure 6e also indicates that the weakly stratified northern water column was again nearly homogenized to beyond the 650-m level by the cooling episode of late March (Fig. 2).

The important role of the eddy exchange is underscored by the deep temperature records (Fig. 7) that show increased variance after convection below the stratification, with the LIW salinity maximum remaining intact. That is the case, for example, for station T2, and also for T3 (Fig. 7), in comparison with the near-surface temperature plots of Fig. 6. The subthermocline migration of convection water masses was also found in the tracer studies on R/V *Poseidon* in late February to early March 1992 of Rhein (1995). As pointed out previously by Schott et al. (1994), comparing convection winters in the Greenland and Mediterranean seas, the increased deep temperature variance can serve as convection indicator in spring or even summer surveys

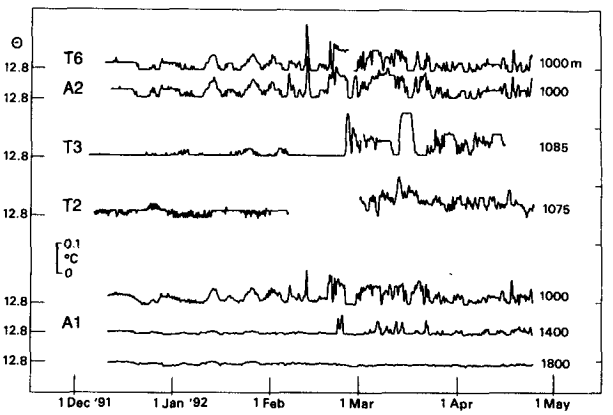

FIG. 7. Time series of deep temperature fluctuations showing increased deep variance after convection.

following convection winters. Further, the deep temperature variability at station A1 was found to be delayed and reduced in amplitude between the 1000 and 1400 m deep records. However, deep temperature variability was absent at 1800-m depth, confirming that convection did not reach that depth. At the southern rim of the convective area, at station T3, enhanced temperature variability was observed several days after the convection period, providing a timescale estimate for the exchange of convection water with the surroundings.

4. Current observations

a. Horizontal currents and mesoscale variability

One objective of the moored array was to investigate changes of mesoscale variability. This might be associated with the decay of the convection regime and water mass exchange with the surroundings as suggested by numerical model results (e.g., Jones and Marshall 1993; Send and Marshall 1995) and scaling arguments (M. Visbeck et al. 1995, unpublished manuscript).

Current vector plots of 40-h low-passed horizontal currents from several depths at the different stations are shown in Fig. 8. Table 1 summarizes the record-length statistics and the fluctuating kinetic energies (FKE) for the period prior to convection (14 December to 31 January) compared to the post-convection period (1 March to 14 April). The record-length mean flow is generally <2 cm s^{-1} and in agreement with cyclonic circulation (Table 1). The dominant period of the variability is one to two weeks, but there are different regimes as regards vertical structure and reaction of the mesoscale currents to the onset of convection. In the center of the dome, at position A1 in the small-scale triangle (Fig. 1), recorded by the two ADCPs above 650 m and by ACMs below, the currents are dominantly in phase between 75 and 2100 m. Amplitudes

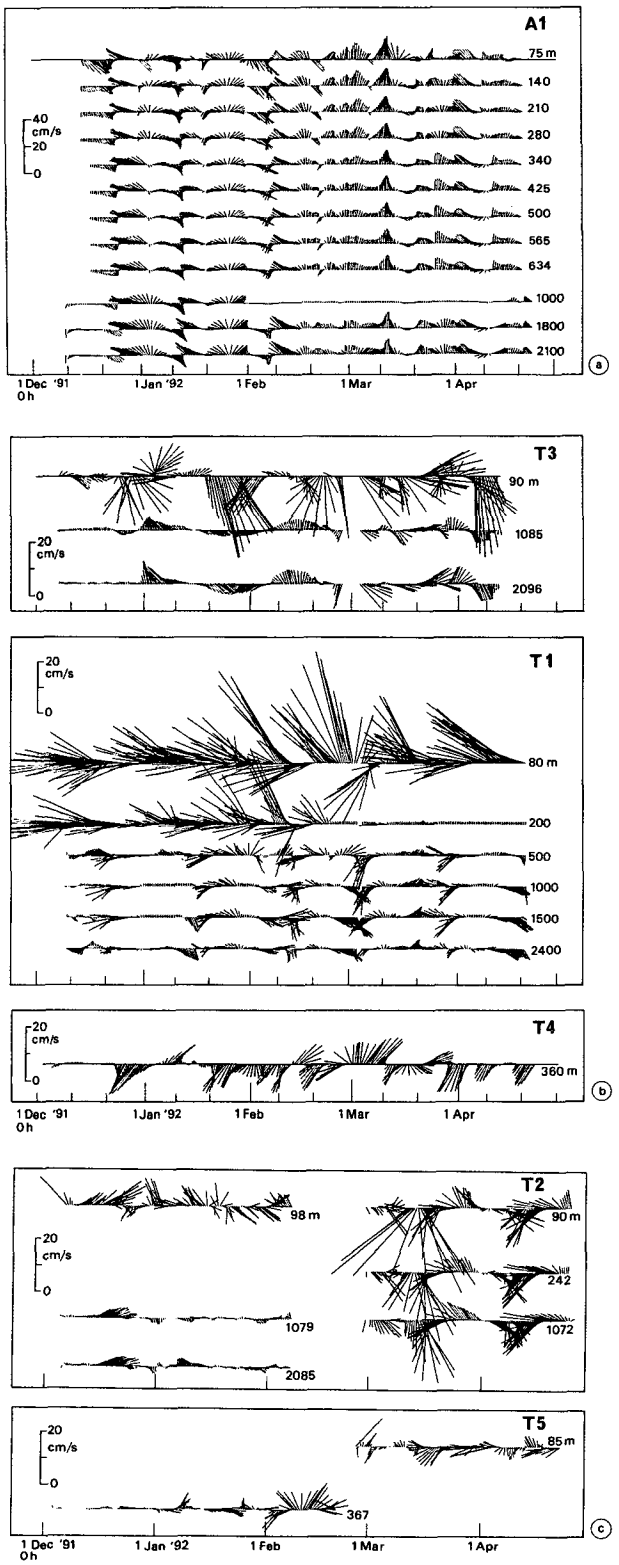

FIG. 8. Horizontal current vector diagrams, with fluctuations < 40 h period removed by Lanczos low pass at (a) station A1; (b) stations T3, T1, T4; (c) stations T2, T5.

decay only slightly in the vertical (Table 1) during the entire recording period (Fig. 8a), independently of the stratification condition (Fig. 6). In the period following deep convection, when mesoscale energy production through baroclinic instability should be occurring, no obvious change is detectable. In fact, the FKEs in the 300–600-m depth range of stations A1, A2, T6 decreased by a factor of 2 between the pre- and the postconvection period, and for the deep currents that factor is similar.

The development is different at the other stations (Fig. 8b). At T3, which was only intermittently located within the convection regime (Fig. 4), and at T1, which was within the northern boundary current (Fig. 1), the near-surface currents were much stronger than, and generally out of phase with, the deep currents (Fig. 8b), indicative of dominantly first-mode structure. At T1 and the deep records of T3, there was a near doubling of deep FKE following convection (Table 1), while in the near surface at T3 there was not much change in surface FKE. At T2, east of the convection regime (Fig. 4), the development was again different: there was a drastic change of structure from baroclinic to near-barotropic in mid-February resulting in a tenfold increase of deep FKE.

The interpretation of the mesoscale currents in terms of their relation to deep convection is hampered by the fact that there exists variability in the wind forcing, for example, due to the mistral events, at timescales of several days to a few weeks (Fig. 2a). This wind variability may generate large background mesoscale current variability independent of convection-generated eddies. Baroclinic instability of the stratified boundary current is also a possible source of mesoscale energy in the convection region.

One likely consequence related to the stratification change caused by deep convection is the decrease of mesoscale variability within the regime, from an average of 48 $cm^2\ s^{-2}$ to half that value for the upper 600 m and from 43 to 14 $cm^2\ s^{-2}$ for the deep sensors (Table 1); and the increase of FKE outside (at stations T2 and T3). However, the correlations between current fluctuations and temperature or salinity were very low. Meaningful eddy transfers related to those changes could, thus, not be derived from the moored measurements.

b. *Vertical velocities and convection*

Unfiltered time series of the vertical velocities from two ADCP records at 212 and 495 m depth at station A1 show distinct bursts of high-frequency vertical velocity variance (Fig. 9) associated with the episodes of cold-air outbreaks of late December and February as described above. The upper-layer record also shows diurnal cycles related to vertical zooplankton migration as observed elsewhere (Fischer and Visbeck 1993).

TABLE 1. Mean and mesoscale horizontal current statistics.

Mooring iD	Depth (m)	Record length (cm s^{-1})					FKE (cm^2 s^{-2})	
		Days	$\bar{u}$	$\bar{v}$	$(\overline{u'^2})^{1/2}$	$(\overline{v'^2})^{1/2}$	14 Dec–31 Jan	1 Mar–14 Apr
				Deep records				
A1-RCM	1000	—		*			35.7	*
A1-RCM	1800	134	−1.2	2.4	5.7	4.4	41.1	14.1
A1-RCM	2100	134	−1.2	2.7	5.8	4.5	51.0	18.7
A2-RCM	1000	—		*			27.4	*
A2-RCM	1800	132	−0.7	1.8	5.7	3.8	41.8	10.8
T6-RCM	1000	133	−0.8	1.5	4.8	3.7	31.1	7.9
T6-RCM	1800	133	−1.1	2.6	6.6	4.9	52.2	18.5
T2-RCM	1075	118	−0.8	−2.0	6.2	5.4	5.9	52.0
T3-RCM	1092	130	0.3	−0.1	2.7	2.8	4.8	8.4
T3-RCM	2096	130	0.9	−0.2	4.5	4.2	11.0	19.0
				Shallow records				
T2-RCM	90	118	−1.3	−1.1	9.9	9.4	75.4	114.6
T3-RCM	90	130	2.3	−6.4	11.3	11.5	143.3	123.5
T4-RCM	360	128	−1.0	−2.3	5.5	6.0	31.0	35.2
A1-ADCP	75	133	−0.7	1.7	9.0	9.2	101.7	62.3
A1-ADCP	340	129	−0.8	1.5	6.2	4.9	40.0	16.1
A2-ADCP	340	140	−0.7	1.6	6.4	5.0	40.3	17.9
T6-ADCP	340	131	−0.8	1.7	6.6	5.9	42.2	21.2
A1-ADCP	634	129	−1.1	1.7	5.9	4.7	37.2	16.0
A2-ADCP	610	140	−1.1	1.6	6.0	4.7	39.0	16.2
T6-ADCP	610	131	−1.0	1.8	6.1	5.0	38.4	17.7
				Stratified boundary current regime				
T1	80	131	−19.0	5.6	10.4	12.3	80.4	135
T1	500	131	−3.1	−0.3	4.7	3.4	11.3	16.8
T1	1000	131	−1.2	−0.5	5.0	2.9	11.8	18.5
T1	1500	131	−0.3	−0.9	5.6	3.1	12.9	21.3
T1	2400	131	0.6	−0.6	3.6	2.0	6.3	9.9

* Partly stalled.
RCM: rotor current meter.

The short-period fluctuations of the late December event are fairly symmetrical up and down motions within the stratification still existing at that time at the 200–500 m level (Fig. 6a). These fluctuations are internal waves that were apparently generated by upper-layer mixing and convection causing pressure fluctuations in the stratified water underneath. Such internal wave variance was also observed by Schott et al. (1993) in early winter within the stratification in the central Greenland Sea. The late February fluctuations, however, have the asymmetric appearance as observed by SL91 during the time of convection: strong downward motions of 5–10 cm s^{-1}, with weaker upward motions in between. Vertical velocity variance of the high-pass filtered fluctuations in Fig. 9 shows some other smaller velocity variance occurrences in addition to the two major events. In contrast to the observations of SL91, where the short-period velocity fluctuations were almost depth independent in the 250–550-m observational range, the vertical velocity variance of the February event decays significantly between 300 and 600-m depth, as shown below.

5. The convection period of 18–23 February

An expanded view of the convection period for the observations of the triangle A1, A2, T6 (Fig. 1) is shown in Fig. 10, together with fluctuations of winds and heat flux components as measured by the shipboard systems of R/V *Poseidon* while working near that array. Strong surface cooling occurred during the night with latent heat fluxes alone amounting to 400 W m^{-2} and total heat flux in excess of 600 W m^{-2} (Fig. 10b). The temperature and salinity records from station A1 show that the convection reached the 1000-m level on 19 February and the 1400-m level on 22 February, but the 1800-m level is not affected (Figs. 10c,d). The fluctuations of temperature and salinity that nearly compensate in density are an indication of the incomplete mixing and advection of different water masses past the mooring site. Application of a Kraus–Turner mixed layer model by Mertens (1994) over the winter of 1991/92 resulted in similar depth development of convection to only intermediate depths.

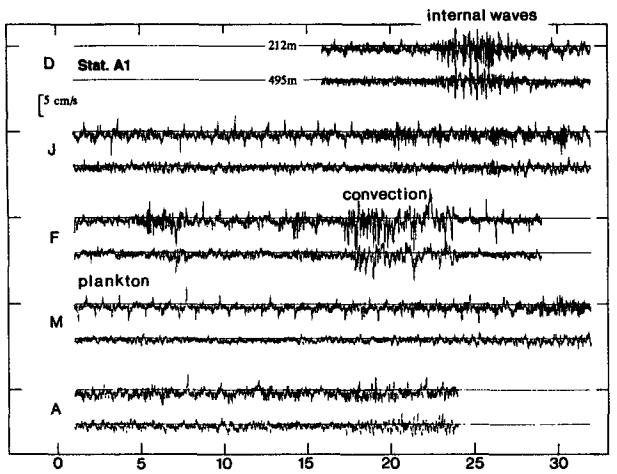

FIG. 9. Vertical velocities recorded at station A1 at 212- and 495-m depth during 17 December 1991–24 April 1992. Particularly recognizable are diurnal plantkton migration, internal waves (December), and convection (late February).

Concerning the horizontal scale of the vertical velocity fluctuations, the interesting result from the simultaneous ADCP measurements at 300–400 m depth in the small-scale array is that they were decorrelated over the 2 km horizontal station distance (Fig. 10e). Previous deductions of their small scale by SL91 and Schott et al. (1993) were based on single station ADCP measurements and the advective timescale of an event. The horizontal currents on the timescale of the plumes were also decorrelated among the stations (Fig. 10f), and meaningful vorticity calculations could not be carried out. Hence, for the plumes, horizontal scales have to be estimated again from the individual station measurements.

The vertical velocity variance at 300–400-m depth ranged from 3.4 to 7.1 $cm^2\ s^{-2}$, and thus was an order of magnitude larger than during the quiet period in March (Table 2), but lower than the 10 $cm^2\ s^{-2}$ obtained from the hourly ADCP observations of SL91 during the mistral of 1987. When using subsets of the 1992 records (at hourly resolution as in 1987), the variances did not change significantly compared to the full dataset, confirming that the observed differences between the two convection events were real rather than due to aliasing in the hourly record of 1987. The high-frequency variance of the 6-h high-pass filtered time series contributed about 40% to the total variance, which is similar to the ratio of the stronger convection event in 1987 (SL91).

Horizontal fluctuating kinetic energies (HFKEs) derived from the unfiltered ADCP dataset did not vary much from the mistral week to the quiet period in March (Table 2; Fig. 8a). However, in the high-frequency band (<6-h period), the HFKE of the convection period was five times larger than during the post-convection phase. This was similar to the 1987 dataset where the HFKE was an order of magnitude larger during the mistral week compared to the preceding (quiet) week. Another similarity between the two datasets (1987, 1992) is the ratio between horizontal and vertical kinetic energy during convection, which in both cases was 4:1, while the absolute values were different (SL91).

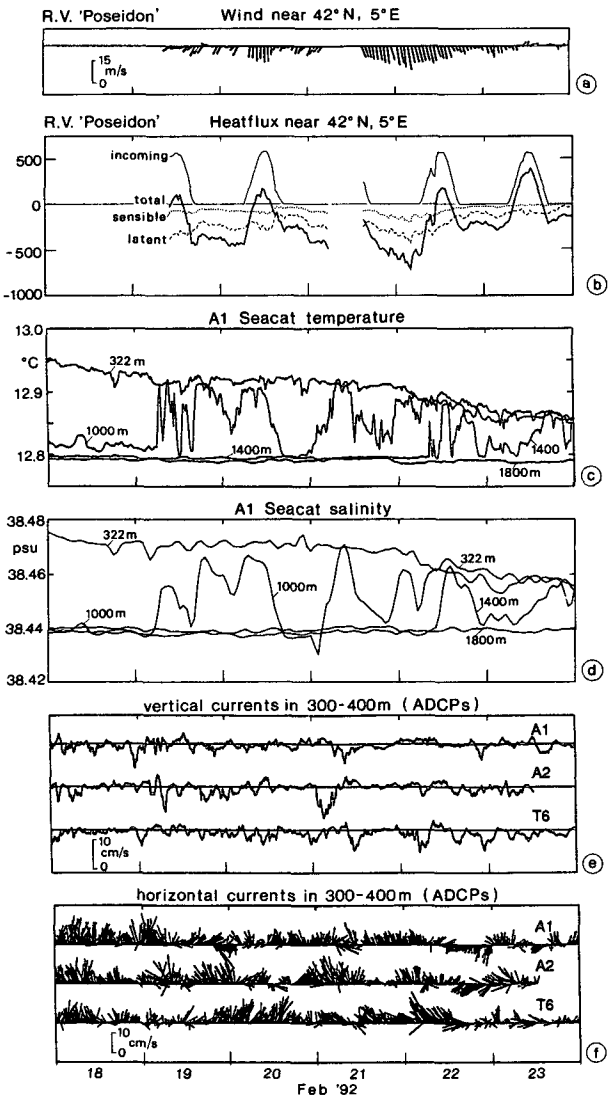

FIG. 10. The convection period of 18–23 February 1992: (a) winds (direction toward) near 42°N, 5°E, recorded by R/V "*Poseidon*"; (b) heat flux from "*Poseidon*" meteorological observations; (c) temperatures at several depths, station A1; (d) salinities at several depths at station A1; (e) vertical velocities at 300–400-m depth from ADCP measurements, stations A1-A2-T6; (f) same as (e) but for horizontal current vectors.

TABLE 2. Means and variances of ADCP currents (bin 2) during 18–23 February (mistral period) and 7–13 March (quiet period).

Profiler	Depth (m)	Record segment	6-h high-pass time filter applied?	Means (cm s^{-1}) $\bar{u}$	$\bar{v}$	$\bar{w}$	$\bar{v}_e$	Variances (cm^2 s^{-2}) $\overline{u'^2 + v'^2}/2$	$\overline{w'^2}$	$\overline{v_e'^2}$
A1U	280	2/18–2/23	n	0.2	3.3	+0.3	−0.6	18.6	4.2	0.2
A1D	340		n	0.1	2.6	−0.1	−0.5	16.3	3.4	0.3
A2	340		n	−1.1	3.3	−0.2	−0.4	17.3	7.1	0.3
T6	340		n	−1.1	3.4	−0.6	−0.4	18.5	5.4	0.3
A1U	280	2/18–2/23	y	—	—	—	0.5	5.6	1.7	0.2
A1D	340		y					8.0	1.7	0.3
A2	340		y					8.5	2.8	0.2
T6	340		y					9.8	2.4	0.3
average		3/07–3/13	n	1.5	6.1	−0.3	−0.5	12.8	0.5	0.2
(without A1U)			y					1.7	0.2	0.1

Figure 11a shows the vertical structure of the vertical velocity fluctuations in the depth range 75–634 m, covering the range of the two ADCPs of station A1. Some velocity events, for example, on 18 February at 2300 UTC, occur almost in phase over the entire range but with an amplitude maximum at 250–350 m. Others, for example, 22 February at 2300 UTC, are limited to an intermediate depth range, decoupled from the upper-layer variance. Horizontal currents from station A1 for the same depths are shown in Fig. 11b. (Note: The ACM rotor at 1000 m had stalled for the entire convection period, and the rotor at 1800 m stalled for part of the time.) Current vectors of the short-period fluctuations show significant vertical structure compared to the near-barotropic nature of the mesoscale variability (Fig. 8a) and also in contrast to the 1987 observations of SL91.

Given the fact that the heat flux over the convection regime, even during the mistral period, shows a pronounced diurnal cycle (Fig. 12a) with heat gain during mid-day, generation of plumes should occur dominantly at night, at maximum buoyancy flux. When plume velocities measured by the four ADCPs during 18–23 February, at 280-m depth for A1U and 340 m for the three downward looking instruments, are displayed versus the time of day, predominance of large plume velocities is detectable during the night and early morning hours (Fig. 12b), resulting in maximum variance, while minimum variance occurs in the afternoon (Fig. 12c). For comparison, the preconvection variance for the same levels, calculated for the period 5–15 February, is also shown in Fig. 12c. The average afternoon variance at convection times is still a factor of 5 larger than prior to convection, or later in March (Table 2).

There is also a significant decrease of plume velocity variance from the 280 to 340 m level to the 634-m level (Fig. 12d). Recall that plume velocities are superimposed on a diurnal plankton cycle (Fig. 9) that is directed upward at about 1800 UTC, explaining the evening peak of the preconvection variance (Fig. 12c) and downward at about 0600 UTC. That the vertical velocity events continue to exist about 6 h after cooling ends (Fig. 12b) sets a lower limit for their lifetime, while the fact that their energy decreases by a factor of 4 between the early morning and afternoon hours suggests that their lifetime is at least not long compared to an inertial period. The decrease of large vertical velocities shortly after the end of the cooling (23 February) is also apparent from the time series in Fig. 9. This timescale bracket indicates the transition from plumes to two-dimensional rotating vortices.

Since the apparent timescale of a plume in the Eulerian measurements (<2 h) is short compared to that lifetime estimate (the order of an inertial period), it may be assumed that plumes are quasi-frozen structures being advected past the observation site by the mean current. The interpretation of the vertical structure of a plume recorded at an individual profiling site then depends on several factors: first, it depends on how the plume is "sliced" by the profiler—that is, close to the center or at one of the sides. Second, a vertical shear of the horizontal mean current may cause the orientation of the plume to be slanted in the water column, and only part of it may be detected by the ADCP. Third, the horizontal scale of a plume compared to the range-dependent separation of the acoustic beams of the ADCP is important, as discussed below.

An important result of the small-scale array concerns the mean vertical motion over the period of convective fluctuations. Averages for the period 18–23 February, after correcting for the vertical velocity bias, were near zero for A1D and A2 and −0.6 cm s^{-1} for T6 at 340-m depth, and 0.3 cm s^{-1} at 280-m depth of A1U (Table 2). This result confirms that the plumes act like mixing agents rather than carrying mean transport downward.

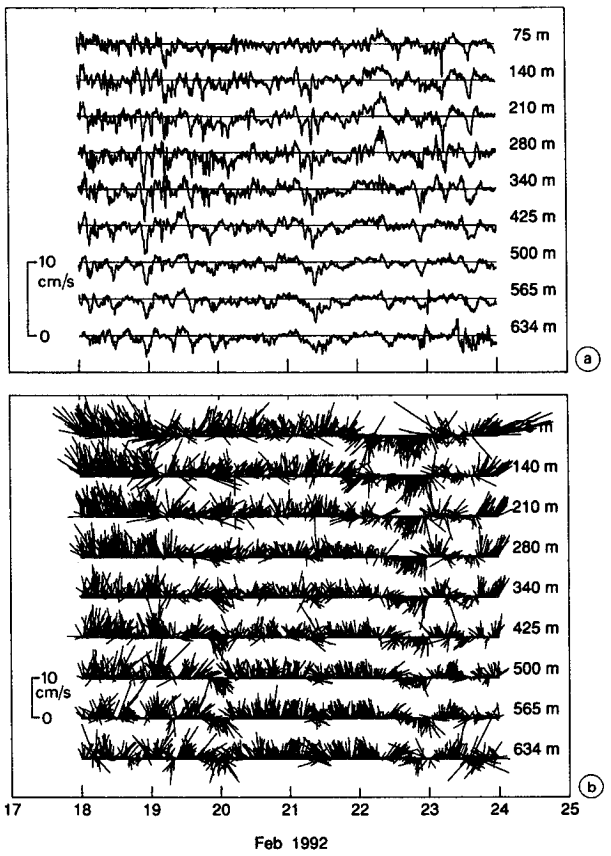

FIG. 11. (a) Vertical velocities in depth range 75–634 m from the two ADCPs at station A1 during the mistral period of 18–23 February. (b) Same as (a) but for horizontal current vectors.

It corresponds to the findings of Schott et al. (1993) for the incomplete mixing case in the Greenland Sea, but differs from the February 1987 result of SL91, where a mean downward motion during the mistral week of 1.0 cm s^{-1} was determined. That a simple one-dimensional mixed layer model reproduced the depth development of the convection quite well also supports the role of the plumes as turbulence elements.

6. Individual convection events

Convective activity at station A1 during 18–19 February is shown in Fig. 13a. Maximum downward velocities exceeded 8 cm s^{-1} during the night, and weaker downward motions occurred subsequently. The scale of the main event of Fig. 13a was estimated at 600 m, based on the horizontal currents shown in Fig. 13b for the same time period, with the vertical velocities superimposed by shading. A second example of weaker convection is shown from 23 February (Fig. 13c), when downward motion occurred over 3 h. The horizontal scale derived from the advection (Fig. 13d) was again estimated at about 500 m.

Visbeck (1993) investigated the plumes with a kinematic model where a radial profile was given for the vertical velocity with downward motion at the center and weaker upward motion outside resulting in a net zero vertical flow constraint for a horizontal layer. Specifying also a vertical profile of the vertical velocity yields divergent horizontal currents due to continuity. Further, rotation of the plumes was allowed for, leading to cyclonic inflow at the top and anticyclonic outflow at depth. Free plume parameters are the cell diameter, the strength of downwelling, and rotation. Further, the location (of the section sliced through the plume by the profiler) and the advection velocity were variable. This kinematical model, when fitted to the ADCP data, including the effect of beam separation, confirmed the simple estimates of horizontal plume scales made above. As regards rotation, the first case (Figs. 13a,b), measured shortly after the beginning of the convection, yielded no detectable rotation while the second case (Figs. 13c,d) yielded cyclonic rotation for the best fit. However, fitting a number of individual plumes for all

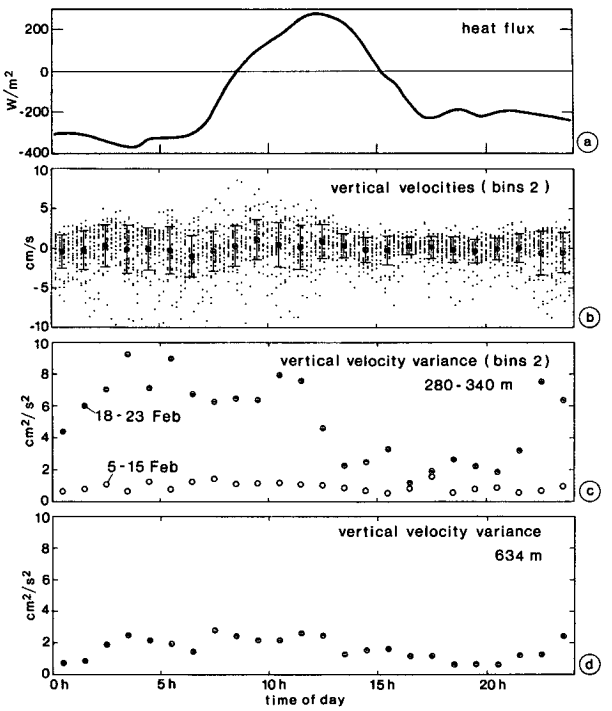

FIG. 12. (a) Mean diurnal heat flux from *Poseidon* shipboard measurements during 18–23 February. (b) Vertical velocities from bin 2 of each of the ADCPs in the small-scale triangle (corresponding to 280 m for A1U, and 340 m for A1D, A2, T6) as well as means and standard deviations, as function of time of day during 18–23 February. (c) Vertical velocity variance for hourly samples of data from (b), full circles, and for the preconvection period, 5–15 February, open circles. (d) Vertical velocity variance at 634-m level from the three downward looking ADCPs during the convection period (18–23 February) as function of time of day.

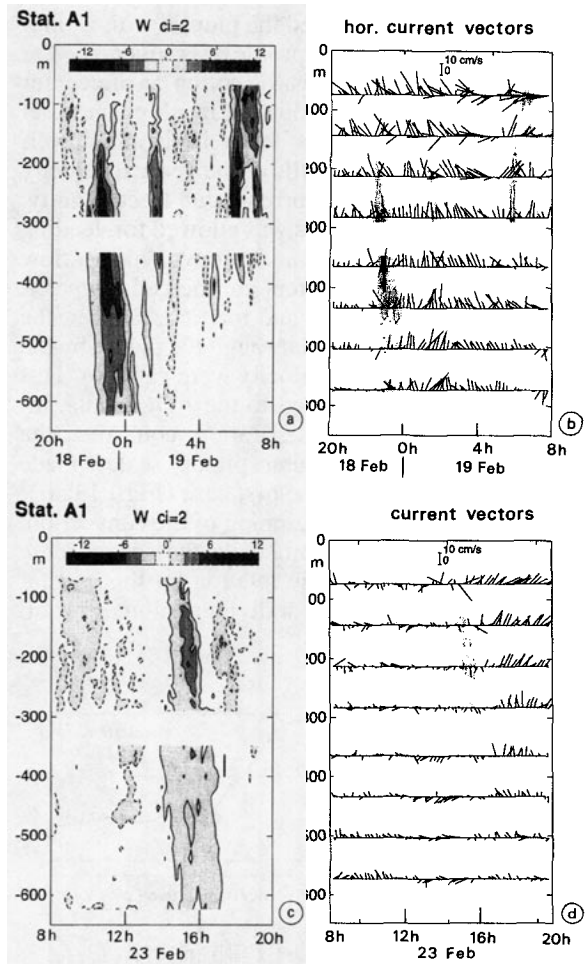

FIG. 13. (a) Contour plot of vertical currents at station A1 during 2000 UTC 18 February to 0800 UTC 19 February; contour interval (indicated by shading, top) is 2 cm s^{-1}; (b) horizontal current vectors for same segment, with convection velocities superimposed by shading; (c) as in (a) but for 0800–2000 UTC 23 February; (d) as in (b) but for 0800–2000 UTC 23 February.

three profilers from the triangle individually did not yield significant trends in the sense and magnitude of plume rotation. It turned out that some combinations of the free parameters were dependent and resulted in nonunique solutions. A smaller size of the moored ADCP triangle might have yielded correlated events among the three profilers and might have eliminated the ambiguity of the fits.

Another way of exploiting the ADCP beam separation for estimating horizontal scales uses the so-called error velocity. While the vertical velocity is the average of all four beam Dopplers, the error velocity is the difference between the two orthogonal beam pairs. It thus is a measure of the inhomogeneity among the beam Dopplers. Hence, for a plume of vertically constant diameter that is comparable to the beam separations, the vertical velocity will decrease with distance from the transducer and the error velocity will increase. This behavior was clearly seen during the convection period 18–23 February in the vertical and error velocity variance (Fig. 14). The vertical velocity maxima at about 300-m depth were located near the transducers of the upward looking ADCP at station A1 and the three downward looking ADCPs at A1, A2, and T6, and decreased with distance from the transducers. For the error velocity, the increase is pronounced in the upward direction (Fig. 14) indicating plume-scale decrease toward the surface, while in the deeper range a constant level is approached, which is probably instrumentally determined.

Using the circular plume model and fitting its diameter to the rms vertical and error velocities for the convection period 18–23 February yielded mean horizontal scales in the upper 100–300 m, from A1U, of about 400 m. In the depth range 300–600 m, the scale increased with increasing depth, from 400 to 600 m, for all three downward looking ADCPs. The tendency for increasing width with depth might suggest that

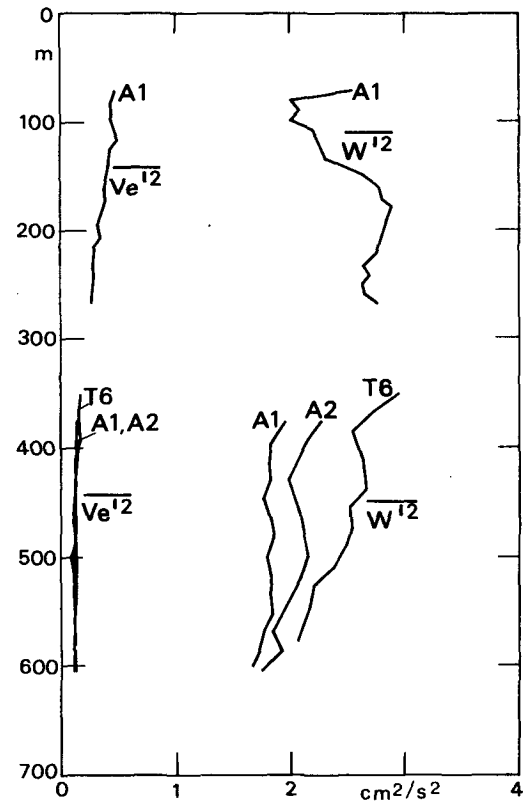

FIG. 14. Profiles of vertical velocity variance ($\overline{w'^2}$) and error velocity variance ($\overline{v_e'^2}$) for the convection period 18–23 February as observed by the upward-looking ADCP at stat A1 in depth range 80–250 m (top) and the three downward looking ADCPs on stations A1, A2, T6.

plumes entrain water from the environment on their way down. A similar conclusion was also drawn by Schott et al. (1993) from the few plumes observed in the Greenland Sea convection area in winter 1988/89. On the other hand, in the individual time series of vertical velocities (Fig. 11a), a depth increase of the convection event durations is not noticeable, which does not support such a drastic depth increase of horizontal plume scale. Besides, the bottom of homogeneous CTD profiles indicate, as discussed above, that plumes also do not seem to entrain at their bottom end. Hence, other effects besides plume kinematics, for example, instrumental noise, could have a bearing on the observed error velocity profile. Further, there could be a genuine decrease of plume velocity between 300- and 650-m depth, as also suggested by the decrease in diurnal cycle vertical velocities at the three instruments (Figs. 12c,d).

7. Adjustment and rim current

Since convected water is trapped by rotation in the deep-mixed regime and cannot escape by flowing out at depth, it has to be horizontally exchanged across the front with the stratified regime around it. The fact that such exchange exists is underscored by the observations of homogeneous water parcels underneath the stratification outside the original convection regime, where the deeper layers were not in direct exchange with the surface at any time during the forcing period. In Fig. 4, an outer regime around the deep convection regime was marked in which intermediate-depth water mass properties corresponded to those observed within the regime at the time of deep convection. These water masses were inhomogeneous within the bounds of the incomplete mixing of the patch. The convected water was also identified by its tracer concentrations (Rhein 1995). The region of convection from hydrographic data (Fig. 4) agrees well with the F12 saturation of 60% (Rhein 1995, Fig. 7b), while the region with homogeneous water parcels underneath the stratification agrees well with the 70% F12 saturation. It is also supported by increased deep temperature variance in the moored records from below the stratification around the convection regime.

Our measurements do not allow a satisfactory interpretation of the mechanism by which the water is exchanged between the convection patch and the stratified surroundings. One of the objectives of the triangular-array measurements was detection of instability eddies that are expected to carry external water mass characteristics into the deep-mixed regime; that is, they should be anticyclonically rotating and should possess an LIW intermediate salinity maximum. A clear identification of such eddies drifting through the array could not be made, due to the background of preexisting mesoscale energy. Although the small triangle was located near the southern front of the convection regime initially, currents there were near-barotropic throughout the deployment period (Fig. 8a). That background energy was probably also the reason why eddy heat and salt flux calculations did not yield sensible results commensurate with cross-frontal exchange. In particular, time series of those fluxes did not show significant changes for the adjustment period after convection compared to the preconditioning time. At T3, just south

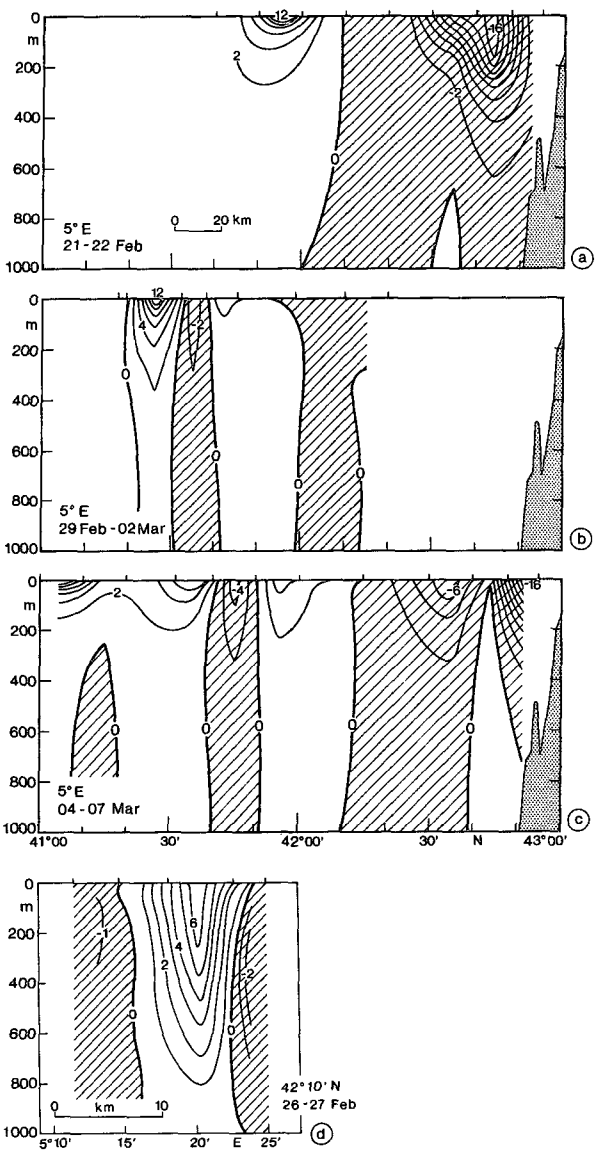

FIG. 15. Geostrophic current (in cm s^{-1}) relative to 1000 dbar from the sections along 5°E by R/V *Poseidon* for (a) 21–22 February 1992 (location, see Fig. 4a); (b) 29 February–2 March 1992 (Fig. 4b); and (c) 4–7 March 1992 (Fig. 4c). Positive flow is eastward; (d) same as (a) but for tow-yo section of 26/27 February across the margin of the convection regime approximately along 42°10′N; positive is northward (location, see Fig. 4b).

of the front, where strong first-modal fluctuations occurred after the convection period, the fluxes were also not in any meaningful relation to anticipated cross-frontal exchanges.

The geostrophic adjustment at the perimeter of the convection regime should cause a rim current around the convection regime, flowing cyclonic on top and anticyclonic at depth (e.g., Madec et al. 1991; Jones and Marshall 1993). At the scale of the Gulf of Lions, a cyclonic rotation does exist, and the boundary array of stations A3, T1 (Fig. 1) was located there to measure transport changes that might occur in conjunction with deep convection. Transport time series were determined from this array and compared well with geostrophic sections at the time of the various ship surveys along 6°E (Schumacher 1994). They showed, however, large transport variations throughout the winter, apparently independent of what happened in the convection regime. At the perimeter of the patch, however, a cyclonic rim current was present. The geostrophic velocity distribution relative to 1000 m from three "Poseidon" sections during the three convection stages presented in Fig. 4 are shown in Figs. 15a–c. For the early stage of convection, a current of 12 cm s^{-1} is observed just south of 42°N (Fig. 15a), located at the rim of the convection region. At the period of deeper convection (Fig. 4b), the section of 29 February to 2 March shows the geostrophic eastward current just south of 41°30′N (Fig. 15b), where the convective water was observed below the stratified surface layer (Fig. 4b). In the tow-yo section of 26–27 February a high-resolution cut across the front (Fig. 4b) separating the two regimes was accomplished, yielding the geostrophic current distribution of Fig. 15d. In the first half of March when no surface convection was observed, the geostrophic eastward current (Fig. 15c) disintegrates into several current bands.

The rim current around the convection regime is apparently of the order of a Rossby radius wide and its magnitude is in agreement with small mean downward motions as predicted from vorticity constraints and similar to that analyzed from a plume-resolving model (Send and Marshall 1995). Its small horizontal scale was not well resolved by the CTD station spacing except by the tow-yos. An attempt to identify it in the shipboard ADCP sections near the front was not successful. It was also not possible to identify it in the moored records of stations T5 and T2, nor at the central triangle A1-A2-T6 that should at certain times have been located close enough to the edge of the convection region to measure a rim current. The mesoscale fluctuations of >20 cm s^{-1} amplitude near the surface and with periods of 1–2 weeks (Fig. 8) would have masked the occurrence of a rim current.

8. Discussion and conclusions

A significant fraction of the Mediterranean outflow through the Straits of Gibraltar of about 0.7 Sv (Bryden et al. 1994) is made up by western Mediterranean Deep Water (WMDW) (e.g., Kinder and Parilla 1987), and the only location for the renewal of WMDW is the Gulf of Lions. How is this water formed and transported out of the convection region? Should there be a measurable mean vertical motion within a convection region? In the week-long ADCP measurements of SL91, a mean downward velocity of 1 cm s^{-1} was recorded and, based on this point measurement, SL91 speculated on a mean downward transport of water masses within the convection regime. Based on conservation of potential vorticity, however, a significant mean downward motion should not occur, as discussed by Send and Marshall (1995), who analyzed the nonhydrostatic plume simulation model of Jones and Marshall (1993) and scaled the relevant physical processes in light of rim current properties. The vertical mean motion obtained there was less than 0.1 cm s^{-1} and corresponded to a mean downward transport of the order of 0.01 Sv (10^6 m^3 s^{-1}) averaged over the year and for a typical convection regime scale. The geostrophic adjustment of the model convection region was the cause of this small downward transport of water mass.

In the convection field experiment described here, our measurements of mean vertical velocities during a week-long convection period were <0.6 cm s^{-1} for the individual ADCPs, after removal of instrument biases. The average downward velocity, for the convection period 18–23 February, over the four closely spaced instruments was −0.15 cm s^{-1}, and thus confirms the principles outlined above. This conclusion was already drawn from convection observations with moored ADCPs in the Greenland Sea by Schott et al. (1993), but due to a small number of plumes and only one convection site, it was not solidly founded. The plume activity during the week of mistral forcing in mid-February was weaker than during the stronger-forcing case of 1987 (SL91). Maximum amplitudes were 5–8 cm s^{-1}, compared to >10 cm s^{-1} in 1987, and vertical velocity variance over the entire plume observation period was around 5 cm^2 s^{-2}, compared to about double that value in 1987.

Regarding the horizontal scale of the plumes, the 2-km sidelength of the triangular array of ADCP moorings was too large, making plume occurrences decorrelated and not permitting the combination of the three station measurements into a joint plume analysis. Horizontal plume scales were estimated at 300 to 500 m from the individual ADCP measurements, based on the horizontal advection and assuming frozen plume structures. This result is in agreement with earlier such estimates (SL91; Schott et al. 1993) and with the plume-scale analyses of Jones and Marshall (1993) and Max-

worthy and Narimoussa (1994). Using the ADCP beam spreading and the error velocities to investigate the plume structure, a tendency for plume diameters to increase with depth in the 300 to 600 m ADCP range was detected. This plume widening could indicate plume entrainment of water from the environment on the way down, as was earlier concluded from Greenland Sea plume observations by Schott et al. (1993). However, other effects than beam spreading versus plume scale could be responsible for the correlation loss among beam Dopplers. At the bottom of plumes, significant entrainment did not take place, since density steps in CTD casts were not observed, even in cases of fairly large, but compensating, steps in T, S properties.

It is currently not clear whether rotation of plumes is to be expected. Jones and Marshall (1993) obtain rotational control of plumes at a mixed layer depth $> 1.25(B/f^3)^{1/2}$, with B = surface buoyancy flux and f = Coriolis parameter, while laboratory experiments suggest much larger depths of order $10(B/f^3)^{1/2}$ before this happens (Coates et al. 1995). For typical Mediterranean conditions, this discrepancy means the difference between 600 and 6000 m. In an analysis with a kinematical plume model that included rotation as a free parameter, a consistent pattern of rotation could not be confirmed from the data. As in the 1987 observations of SL91, some plumes were found to rotate cyclonic in the upper part, but others did not.

The deep mixing of early 1992 was found to be incomplete, in so far as significant horizontal property gradients continued to exist, again different from the near-complete mixing case of 1987 (LS91). Overall, a combination of vertical velocity measurements by ADCPs and simultaneous temperature measurements should allow vertical heat flux determinations useful for budgeting the convection regime. However, due to the inhomogeneities that were advected, such calculations did not produce useful results on the vertical fluxes.

While in the past few years the role of plumes as mixing agents was predicted from scale and model analyses and is confirmed by our observations, the further fate of a regime of convected water is still very much unclear and open to speculation. Recent efforts in understanding the role of mesoscale baroclinic eddies in convection regions (Visbeck et al. 1995) have shown that for some idealized scenarios baroclinic eddies can balance the surface buoyancy loss completely. They transport stratified fluid from the rim current region into the chimney and convected water outwards and away below. This rearranging of water masses is consistent with the observed rapid restratification at the surface (Send et al. 1995) and also with the spreading of convected tracer-rich water below (Rhein 1995). However, the role of the mesoscale fluxes in exchanging convection water with the surroundings could not be quantified from the moored and shipboard observations, due to a strong background of mesoscale variability that existed independently of convection. The background mesoscale variability could be generated directly by wind forcing or through baroclinic instability of the stratified cyclonic boundary current around the Gulf of Lions.

In earlier observations of boundary current transports east of the convection regime, Astraldi and Gasparini (1992) reported a relation between increased transports and increased winter heat loss over the Gulf of Lions (estimated from coastal station data), which would suggest a large-scale coupling of the cyclonic circulation to convection activity. The current-meter array we had deployed across the boundary current south of Toulon (Fig. 1) to observe such relations could not detect a convection-related transport signal over the background of preexisting boundary current variability. Instead, indications of a narrow cyclonic rim current, of <20 km width, around the convection regime were found in geostrophic current profiles with near-surface velocities of about 10 cm s^{-1}. This is in agreement, through the vorticity constraint, with the weak downward motion observed by the ADCPs within the regime.

Acknowledgments. We thank captains and crews of the research vessels *Le Suroit, Poseidon,* and *Valdivia* for their cooperation during the field experiment and the director and staff of the IFREMER base in Toulon, which served as staging area for the experiment. Our particular appreciation is extended to C. (''*Monsieur Charles*'') Limonier of IFREMER Toulon, who helped us in every possible way during port stays and equipment exchanges. Dr. J. Font of the University of Barcelona leant us current meters and mooring equipment for the experiment, which is much appreciated. We further thank C. Mertens and G. Krahmann for help in the data analysis. Funding of the THETIS experiment was through EC/MAST, Contract MASTI-CT90-0008, and of the convection studies also by the German BMFT, Contract 03R617-3.

REFERENCES

Anati, D. A., 1971: On the mechanism of the deep mixed layer formation during MEDOC'69. *Cah. Oceanogr.*, **23,** 427–443.

Astraldi, M., and G. P. Gasparini, 1992: The seasonal characteristics of the circulation in the north Mediterranean Basin and their relationship with the atmospheric–climatic conditions. *J. Geophys. Res.*, **97**(C6), 9531–9540.

Bryden, H. L., J. Candela, and T. H. Kinder, 1994: Exchange through the Strait of Gibraltar. *Progress in Oceanography,* Pergamon, Vol. 33, 201–248.

Coates, M. J., G. N. Ivey, and J. R. Taylor, 1995: Unsteady, turbulent convection into a rotating linearly, stratified fluid: Modeling deep ocean convection. *J. Phys. Oceanogr.*, **25,** 3022–3050.

Fischer, J., and M. Visbeck, 1993: Seasonal variation of the daily zooplankton migration in the Greenland Sea measured with ADCPs. *Deep-Sea Res.*, **40,** 1547–1557.

Garrett, C., R. Outerbridge, and K. Thompson, 1993: Interannual variability in Mediterranean heat and buoyancy fluxes. *J. Climate,* **6,** 900–910.

Gascard, J.-C., 1973: Vertical motions in a region of deep water formation. *Deep-Sea Res.,* **20,** 1011–1027.

——, 1978: Mediterranean deep water formation baroclinic instability and oceanic eddies. *Oceanol. Acta,* **1,** 315–330.

Jones, H., and J. Marshall, 1993: Convection with rotation in a neutral ocean: A study of open-ocean deep convection. *J. Phys. Oceanogr.,* **23,** 1009–1039.

Kinder, T. H., and G. Parilla, 1987: Yes, some of the Mediterranean Outflow does come from great depth. *J. Geophys. Res.,* **92,** 2901–2906.

Leaman, K. D., and F. Schott, 1991: Hydrographic structure of the convection regime in the Golfe du Lion. *J. Phys. Oceanogr.,* **21,** 575–598.

Madec, C., M. Chartier, P. Delecluse, and M. Crepon, 1991: A three-dimensional numerical study of deep water formation in the northwestern Mediterranean Sea. *J. Phys. Oceanogr.,* **21,** 1349–1371.

Martel, L., and F. Martel, 1994: Air–sea fluxes and winds over the western Mediterranean Sea from three data set: FNOC, Peridot 1988–1989, Peridot 1991–1992. CETIIS Tech. Rep., 26 pp plus figures.

Maxworthy, T., and S. Narimousa, 1994: Unsteady, turbulent convection into a homogenous, rotating fluid, with oceanographic applications. *J. Phys. Oceanogr.,* **24,** 865–887.

MEDOC Group, 1970: Observation of formation of deep water in the Mediterranean Sea, 1969. *Nature,* **227,** 1037–1040.

Mertens, C., 1994: Winterliche Deckschichtentwicklung und ihre zwischenjährliche Variabilität im nordwestlichen Mittelmeer. M.S. thesis, Faculty of Mathematics and Natural Sciences, University of Kiel, 65 pp.

Rhein, M., 1995: Deep water formation in the western Mediterranean. *J. Geophys. Res.,* **100**(C4), 6943–6959.

Schott, F., and K. D. Leaman, 1991: Observations with moored acoustic Doppler current profilers in the convection regime in the Golfe du Lion. *J. Phys. Oceanogr.,* **21,** 558–574.

——, M. Visbeck, and J. Fischer, 1993: Observations of vertical currents and convection in the central Greenland Sea during the winter of 1988/89. *J. Geophys. Res.,* **98**(C8), 14 401–14 421.

——, ——, and U. Send, 1994: Open ocean deep convection, Mediterranean and Greenland Seas. *Ocean Processes in Climate Dynamics: Global and Mediterranean Examples,* P. Malanotte-Rizzoli and A. R. Robinson, Eds., Kluwer Academic, 203–225.

Schumacher, J., 1994: Zirkulation im Golf von Lion im Winter 1991/92 in Zusammenhang mit winterlicher Konvektion. M.S. thesis, Faculty of Mathematics and Natural Sciences, University of Kiel, 74 pp.

Send, U., and J. Marshall, 1995: Integral effects of deep convection. *J. Phys. Oceanogr.,* **25,** 855–872.

——, F. Schott, F. Gaillard, and Y. Desaubies, 1995: Observation of a deep convection regime with acoustic tomography. *J. Geophys. Res.,* **100**(C4), 6927–6941.

Swallow, J. C., and G. F. Caston, 1973: The preconditioning phase of MEDOC 1969. Part I: Observations. *Deep-Sea Res.,* **20,** 429–448.

The THETIS Group (F. Schott, U. Send, G. Krahmann, C. Mertens, M. Rhein, M. Visbeck, Y. Desaubies, F. Gaillard, T. Terre, J. Papadakis, M. Taroudakis, G. Athanassoulis, and E. Skarsoulis), 1994: Open-ocean deep convection explored in the Mediterranean. *Eos, Trans. Amer. Geophys. Union,* **75,** 217–221.

Visbeck, M., 1993: Konvektion im offenen Ozean. Interpretation von Beobachtungen aus der Grönlandsee und dem westlichen Mittelmeer. Inst. Meereskd. Report No. 237.

——, J. Marshall, and H. Jones, 1995: On the dynamics of convective chimneys in the ocean, submitted.